1. INTRODUCTION

NASA's Mission to Planet Earth (MTPE) is engaged in the study of changes in our global environment, and mankind's role in such changes. Taking advantage of the unique perspective available from space, instruments on research satellites launched by NASA are being used to observe and assess large-scale environmental processes, with an emphasis on climate change. MTPE satellite data, complemented by aircraft and ground data, will enable us to better understand environmental changes, to determine how human activities have contributed to these changes, and to understand the consequences of such changes.

In support of the MTPE goals, NASA plans to launch the Advanced Microwave Scanning Radiometer (AMSR) on its Earth Observing System (EOS) PM-1 satellite in late 2000. The PM-1 AMSR is a passive microwave instrument modified from the AMSR originally designed and built by Mitsubishi Electronics Corporation for deployment on the Japanese Advanced Earth Observing Satellite-II (ADEOS-II). From AMSR brightness-temperature measurements a variety of geophysical variables can be estimated describing the states of the atmosphere, ocean, cryosphere, and land-surface. Our investigation focuses on estimation of three land surface variables: surface soil moisture (or soil "wetness"), m_e; land-surface temperature, T_e; and vegetation water content, w_e. These variables will be derived as Level 2 products, and will be the deliverable "EOS Standard Products" of this investigation. This document describes the physical models, retrieval algorithm, processing procedures, and validation approach for generating and evaluating these products. The data products will be used for a variety of research and operational purposes, including surface energy and water balance studies, large-scale hydrologic modeling, numerical weather prediction, climate modeling, and monitoring of floods, land-cover change, droughts, and other climatic anomalies. These studies are central to the "Seasonal-to-Interannual Climate Variability and Prediction" and "Natural Hazards" research objectives of NASA's MTPE program, and will contribute also to the "Land-Cover and Land-Use Change" and "Long-Term Climate" research objectives.

The procedure for deriving the variables m_e, T_e, and w_e from AMSR data is based on a simplified, but state-of-the-art, physical model of microwave emission from a layered soil-vegetation-atmosphere medium. The forward model is nonlinear, hence an iterative, least-squares-minimization inversion method is employed in the retrieval algorithm. The retrieved variables represent area-averages comensurate with the 6.9-GHz AMSR footprints. In addition, the retrievals of m_e and T_e represent weighted averages over a vertical sampling depth in the soil and/or vegetation. Some parameters of the physical model cannot be measured, but are estimated from physical principles or derived empirically a-priori. All parameters are assigned uncertainty estimates, enabling an overall estimate to be made of the geophysical-variable retrieval uncertainties. As the vegetation cover increases, the retrieval errors for m_e and w_e also increase. For dense vegetation these variables cannot be retrieved. The retrieval algorithm is rapid and robust however, and correctly identifies when the reliability threshhold has been exceeded. This has been demonstrated using the current version of the algorithm on historical Nimbus-7 SMMR data, which has similar low-frequency channels to AMSR. Enhanced versions of the algorithm, to

be ready at launch, will have the capability to incorporate ancillary data from external sources, to aid in initializing and constraining the retrieval algorithm. The present version is a stand-alone algorithm, however, and does not assume any externally provided input. As part of this investigation, soil- and atmospheric-model data assimilation will be used to develop higher-level derived products, such as vertical moisture and temperature gradients in the soil, and energy fluxes at the land surface. All products of this investigation will conform to EOSDIS standards and guidelines.

2. OVERVIEW AND BACKGROUND

Routine, global measurements of soil moisture, and a better understanding thereby of large-scale land-surface hydrologic processes, are high priorities for MTPE and EOS. Earth system modeling studies depend on the availability of soil moisture information for initializing and validating atmospheric general circulation models and soil hydrologic models. No other EOS or MTPE mission sensor will provide this measurement.

Measurements of land-surface temperature and vegetation dynamics are needed for surface-flux process studies, and climate and ecosystem modeling. AMSR measurements of these variables will complement similar measurements using optical and thermal infrared sensors on EOS (e.g. MODIS and AIRS). Although passive-microwave measurements are of lower spatial resolution, they are less affected by aerosols and clouds, and are responsive to different dynamic ranges of vegetation structure and biomass than are optical and infrared measurements. There is potential for improved synergistic products of temperature and vegetation using combined microwave, infrared, and optical data.

Vegetation dynamics, surface temperature, and surface wetness (soil moisture) are three of the twenty-four measurement areas identified as high-priorities by the MTPE program (MTPE, 1996). *The AMSR-derived products generated by this investigation,* w_e, T_e, and m_e, *will address directly and uniquely these three critical areas.*

Several studies during the past few years have investigated the influence of land-surface soil moisture on the atmospheric boundary layer (e.g. Brubaker and Entekhabi, 1996) and have provided insights into the importance of soil moisture in controling the feedbacks between land surface and atmosphere that influence climate (Shukla and Mintz, 1982; Delworth and Manabe, 1989). Improved characterizations of land-surface soil moisture, temperature, and vegetation states in numerical weather-prediction models have been shown to provide significant improvement in forecast skills. For example, the large impact of wet versus dry soil moisture conditions on 30-day precipitation forecasts using the European Centre for Medium-range Weather Forecasts (ECMWF) model is shown in Figure 1 (Beljaars et al., 1996). The lack of a global observational capability to provide information on the time and space variations of the moisture, temperature, and vegetation surface states is a major impediment to progress in these fields. The land-surface products provided by AMSR will fill an important gap in the suite of MTPE/EOS measurements.

The terminologies and parameterizations used in describing the surface states are not well defined or consistently applied. The term "soil wetness" is often used to describe the amount of soil water computed from a land-surface model, i.e. a soil-vegetation-atmosphere (or "SVAT") moisture- and heat-flux scheme, with given atmospheric forcing. However, the soil wetness, so defined, is model-dependent—different SVAT models can give different values of soil wetness while having similar estimates of water and energy exchange. Also the soil depth within which the soil wetness is defined varies according to the model (Wei, 1995). When referring to land-surface temperature, the terms "canopy temperature", "skin temperature", "aerodynamic temperature", and "radiation temperature" may be implied, according to the context. This depends on the SVAT model being used, the viewing direction and wavelength of the sensor, and the 3-dimensional characteristics of the surface (Norman and Becker, 1995). Similarly, various parameters have been used to describe vegetation state, including "biomass", "leaf-area index" (LAI), "normalized difference vegetation index" (NDVI), etc. In this document we will define the meanings of the AMSR-derived variables m_e, T_e, and w_e, and indicate how they may be related to some of the definitions above. As part of the research planned in this investigation, techniques will be developed to relate the AMSR-derived variables directly to those required by hydrologic model and land-surface parameterization schemes, and numerical weather prediction models.

2.1 EXPERIMENTAL OBJECTIVE

The objective of this investigation is to provide global, remotely-sensed, land surface products (in regions not covered by snow or ice) of use to the MTPE research and operational forecasting communities. The key land-surface variables that can be derived from AMSR data are the surface soil moisture, m_e, the land-surface temperature, T_e, and the vegetation water content, w_e. Soil moisture has been considered the primary measurement objective of this investigation for EOS. However, surface temperature and vegetation water content must also be estimated, simultaneously, as required corrections in the soil moisture retrieval procedure. Furthermore, as mentioned earlier, these variables are high-priority requirements in their own right for climate and ecological modeling and monitoring purposes. The primary objectives of this investigation can thus be summarized as follows:

- Derive a self-consistent set of the land-surface geophysical variables, m_e, T_e, and w_e, globally (where feasible, as limited by dense vegetation), from the EOS PM-1 AMSR data. These variables will be estimated at a spatial resolution of approximately 70 km (equivalent to the spatial resolution of the lowest AMSR frequency) on a swath-sampled basis. These will be Level 2 Standard Products. Provide accuracy estimates for these geophysical variable estimates.

- Validate the accuracies of the Level 2 products during the post-launch validation phase, and document the algorithms, caveats, and data descriptions necessary for other researchers to utilize the data quantitatively in subsequent scientific studies.

- Make the Level 2 data products, algorithms, and metadata available publicly through EOSDIS.

- Demonstrate the utility of the derived products for: (a) improved understanding of large-scale land-surface hydrologic processes; (b) validating and initializing climate and weather prediction models; and (c) monitoring land surface change and climatic anomalies (including floods and droughts).

2.2 HISTORICAL PERSPECTIVE

To date, rather limited attention has been paid to the use of spaceborne passive-microwave data for land sensing. Previous and existing spaceborne microwave radiometers have been considered sub-optimal, in terms of spatial resolution and frequency range, particularly for soil moisture sensing. The Scanning Multichannel Microwave Radiometer (SMMR), launched on the Nimbus-7 satellite in 1978, had a spatial resolution of ~140 km at its lowest frequency of 6.6 GHz. The Special Sensor Microwave Imager (SSM/I), launched in 1987 has a lowest frequency of 19.3 GHz, at which even small amounts of vegetation mask the surface soil moisture signal. The SMMR and SSM/I were designed primarily for oceanic, atmospheric, and cryospheric studies. Low frequencies (~1 to 3 GHz) are preferable for soil moisture sensing, since attenuation through vegetation is less at longer wavelengths, and the sensitivity to moisture through the top few centimeters of soil is greater at lower frequencies. Notwithstanding this, as discussed below, the 6.6 and 10.7 GHz channels of the SMMR (similar to the low-frequency AMSR channels) have been shown to be sensitive to surface soil moisture under low-vegetation conditions. The improved spatial resolution provided by AMSR (~70 km) is reasonably well-matched to the grid scales of the global atmospheric general circulation models (~50-100 km). The comparative performance characteristics of the SMMR, SSM/I, and AMSR are shown in Table 1 (the EOS AMSR instrument is described further in Section 2.3).

The potential of the 6.6 and 10.7 GHz channels of the SMMR for soil moisture monitoring was first investigated by Wang (1985) and Njoku and Patel (1986). These studies were followed by others (Owe et al., 1988; Choudhury and Golus, 1988; Kerr and Njoku, 1990; Owe et al., 1992; and van de Griend and Owe, 1994). The SMMR was also shown to be useful for monitoring seasonal flooding (Sippel et al., 1994; others), and for vegetation monitoring (Choudhury et al., 1987; Calvet et al., 1994). McFarland et al. (1990), Calvet et al. (1994), and Njoku(1995a) showed that SMMR and SSM/I data can be used to estimate surface temperature. The effects of the intervening atmosphere on land-surface measurements were investigated by Choudhury et al. (1992) and Kerr and Njoku (1993). These studies, and others, have shown the feasibility and potential of future AMSR data for land research.

Table 1: Comparative operating characteristics of SMMR, SSM/I, and AMSR

Parameter	SMMR (Nimbus-7)	SSM/I (DMSP)	AMSR (EOS)
Frequencies (GHz)	6.6, 10.7, 18, 21, 37	19.3, 22.3, 37, 85.5	6.9, 10.7, 18.7, 23.8, 36.5, 89
Altitude (km)	955	860	705
Antenna size (m)	0.79	0.6	1.6
Incidence angle (deg)	50.3	53.1	55
Footprint size (km)			
at 6.6 GHz	140	N/A	70
at 37 GHz	27	35	14
Swath width (km)	780	1400	1445
Launch date	(1978—No longer operating)	(1987—Series in orbit)	2000

Soil Moisture and Flooding

Estimates of large-scale surface soil moisture for comparison with satellite observations can be derived from precipitation and surface meteorological data coupled with models of surface energy and water balance. Such estimates are currently available as forecast outputs of atmospheric general circulation models using four-dimensional data assimilation. An earlier, much-simplified implementation of this approach was the Antecedent Precipitation Index (API), which has been used commonly as an indicator of soil wetness. Shown in Figure 2(a) are SMMR brightness temperatures, T_B, at 6.6 GHz horizontal polarization over two regions in Kansas and Texas plotted as a function of API for five years of data between the months of May and August (Choudhury and Golus, 1988). The relationship between API and T_B is clearly shown. The Texas region (Quadrant (1,3)) has less vegetation and hence the data show a steeper slope (greater sensitivity to surface moisture).

A different model was used by Owe and van de Griend (1990) to estimate large-area soil moisture from precipitation measurements in Botswana (Figure 2(b)). Figure 2(c) shows their comparisons of SMMR-derived surface emissivity at 6.6 GHz versus soil moisture, using corrections for vegetation obtained using AVHRR Normalized Difference Vegetation Index (NDVI) data (van de Griend and Owe, 1994). These comparisons have some limitations. The model-based surface soil moisture estimates rely on sparsely-sampled precipitation data and may not represent well the moisture conditions in the top few centimeters of soil at the time of the

satellite overpasses. Nevertheless, fairly good correlations are obtained between the spaceborne microwave observations and the surface soil moisture. Improved algorithms can be used to account for vegetation in a physically-based manner using multichannel microwave data (as shown later herein), without the need for empirical fine-tuning and ancillary NDVI data in each specific region.

Surface Temperature

Microwave surface temperature retrievals have been tested in limited case-studies using linear regression algorithms developed for SSM/I (e.g. McFarland et al., 1990). Comparison data used by McFarland et al. were surface air-temperatures obtained in the early morning hours close to the times of the satellite overpasses. Accuracies of 2 to 2.5°C were obtained (Figure 3(a)) which were supported by results of simulation studies (Njoku, 1995a) (Figure 3(b)). Practical retrieval algorithms for global application must take into account the vertical and horizontal temperature variabilities that exist at the heterogeneous vegetation/soil surface. Microwave radiometer footprint-average temperature retrievals will be most accurate and easy to interpret for homogeneous surfaces (bare soil or fully vegetated), and less easy to interpret for footprints containing comparable fractions of vegetation and bare soil (Njoku et al., 1995b). Nonlinear effects of vegetation on brightness temperature result in bias errors when using linear retrieval algorithms, thus nonlinear retrieval methods are preferred for global algorithms applicable over a wide dynamic range of vegetation biomass. This is the approach used in this investigation.

Surface Vegetation

Vegetation studies using spaceborne microwave radiometry have been limited mainly to use of a qualitative index consisting of the difference, ΔT, between vertically and horizontally polarized brightness temperatures at 37 GHz (Choudhury et al., 1987; Townshend et al., 1989). This index is simple to use, and the higher spatial resolution available at 37 GHz versus the lower-frequency channels of the SMMR and SSM/I, is advantageous. However, the index is not easily related to a physically-based vegetation quantity. The vegetation opacity, on the other hand, is a parameter of the radiative transfer equation, and is approximately linearly related to the vegetation water content in the 1 to 10 GHz range. Thus, it is possible to make quantitative estimates in this frequency range of the vegetation water content (which is related to the vegetation biomass). It is also important to use the lower frequencies (~6 and 10 GHz), rather than 37 GHz, in estimating vegetation parameters in order to cover a larger dynamic range of vegetation without saturation.

Heterogeneous Surfaces

The effects of mixed surface types within the sensor footprints must be taken into account in microwave retrievals and their applications, due to the heterogeneity of land surfaces. Retrievals of surface parameters from the observed brightness temperatures represent footprint-averaged quantities which are nonlinear area-weighted averages of the component quantities making up the scene— except in the case where vegetation is low, in which case the area-weighted averages are approximately linear (Njoku et al., 1995b). The difference between linear and nonlinear weighted averages is only significant, however, where two dominant components with large contrasts fill the

Table 2. EOS Product Levels

LEVEL	DEFINITION
0	Raw instrument data at full resolution
1	Unpacked or calibrated instrument data at full resolution
2	Derived geophysical parameters at the same resolution as Level 1 data
3	Derived geophysical parameters mapped on uniform space-time grid scales, typically an Earth-located grid
4	Derived geophysical parameters based on models and other products from one or more instruments

footprint in approximately equal amounts. The question of how averaging affects the usefulness of the estimates is a somewhat different (though related) issue, and depends on the flux parameterization schemes of the land-surface models. Much attention has been paid to this aspect recently (e.g. Lhomme et al., 1994; Raupach and Finnigan, 1995), and collaborations with ongoing land-surface modeling investigations and projects, such as the Project for Intercomparison of Land-surface Parameterization Schemes (PILPS), will be pursued as part of this investigation.

Integration of Retrievals with Soil-Vegetation Modeling

Recent studies have considered approaches in which microwave radiances are assimilated directly into predictive models of moisture and heat flow in soils and ecosystem functioning (Entekhabi et al., 1994; LoSeen et al, 1995). Coupled microwave radiative transfer and soil/vegetation heat- and moisture-flux model algorithms can be used to retrieve higher-level products, such as subsurface soil moisture and temperature profile information (as opposed to surface-only values) and surface heat fluxes. While such products are currently exploratory, research will be performed as part of this investigation to develop these products for evaluation purposes (they will be developed initially for application in bare or sparsely-vegetated regions).

An activity has also been initiated by the Principal Investigator of this investigation (E. Njoku), as part of a separate soil moisture study, to collaborate with the National Center for Environmental Prediction (NCEP) in developing techniques for assimilation of microwave-derived soil moisture information into the operational forecast models (F. Chen, personal communication, 1996). This work will involve linkage of microwave-derived surface soil moisture estimates to root zone soil moisture, and comparison of model-forecast surface moisture fields with microwave-derived fields.

2.3 INSTRUMENT CHARACTERISTICS

2.3.1 Instrument Description

AMSR is a twelve-channel, total-power, passive-microwave system that measures brightness temperature at 6.925, 10.65, 18.7, 23.8, 36.5, and 89.0 GHz. Vertical and horizontal polarization measurements are made at all frequencies. The EOS AMSR instrument is a modified version of the design developed for the ADEOS-II AMSR, and consists of a 1.6-m-diameter offset parabolic reflector, fed by an array of six feedhorns. The reflector and feedhorn array are mounted on a drum which contains the radiometers, digital data subsystem, mechanical scanning subsystem, and power subsystem. The reflector/feed/drum assembly is rotated about the axis of the drum by a coaxially-mounted bearing and power-transfer assembly. All data, commands, timing and telemetry signals, and power pass through the assembly on slip-ring connectors to the rotating assembly.

A cold-sky reflector and a warm load are mounted on the transfer-assembly shaft and do not rotate with the drum assembly. They are positioned off-axis such that they pass between the feedhorn array and the parabolic reflector once each scan. The cold-sky reflector reflects cold sky radiation into the feedhorn array. This, and the warm load, serve as calibration references. Corrections for antenna pattern spillover and cross-polarization effects are incorporated in the Level 1 data processing algorithms (see Table 2 for a generic definition of the EOS product levels).

The AMSR rotates continuously about an axis parallel to the local spacecraft vertical at 40 rpm (i.e. with a period of 1.5 s). At an altitude of 705 km, it measures the upwelling scene brightness temperatures over an angular sector of ± 61° about the sub-satellite track, resulting in a swath width of 1445 km. During the period of 1.5 seconds the spacecraft sub-satellite point travels 10 km. Even though the instantaneous fields-of-view are different for each channel, active scene measurements are recorded at equal intervals of 10 km (5 km for the 89 GHz channels) along the scan. The half-cone offset angle of the reflector is 47.4° which results in an Earth-incidence angle of 55°. Tables 1 and 3 list the pertinent performance characteristics.

2.3.2 Calibration

Table 3. PM-1 AMSR Nominal Performance Characteristics

Center Frequencies (GHz)	6.925	10.65	18.7	23.8	36.5	89.0
Bandwidth (MHz)	350	100	200	400	1000	3000
Sensitivity (K)	0.3	0.6	0.6	0.6	0.6	1.1
IFOV (km x km)	76 x 44	49 x 28	28 x 16	31 x 18	14 x 8	6 x 4
Sampling Rate (km x km)	10 x 10	10 x 10	10 x 10	10 x 10	10 x 10	5 x 5
Integration Time (ms)	2.6	2.6	2.6	2.6	2.6	1.3
Main Beam Efficiency (%)	95.3	95.0	96.3	96.4	95.3	96.0
Beamwidth (degrees)	2.2	1.4	0.8	0.9	0.4	0.18

The accuracy of the AMSR brightness temperature measurement includes the rms accuracy, or sensitivity, ΔT, and the absolute calibration accuracy. The sensitivity per sample for each frequency is shown in Table 3, and is a function of the receiver noise temperature, integration time, and bandwidth.

The radiometer calibration accuracy budget, exclusive of antenna pattern correction effects, is comprised of three major contributions: a warm load reference error, a cold load reference error, and radiometer nonlinearities and errors. Accounting for all errors, the total estimated sensor bias error is 0.66 K at 100 K, and increases slightly with temperature to 0.68 K at 250 K.

The major part of the warm-load reference error comes from the following four components: (a) the accuracy of the platinum resistance thermistors (PRTs) as measured by the manufacturer—on of the order of ± 0.1 K; (b) the temperature gradient over the load area (the SSM/I gradient reached values as high as ±0.4 K); (c) load–feedhorn coupling errors due to the design of the system; and (d) reflections out of the feedhorn due to receiver electronics. An estimate of the warm load reference error, taking the root-sum-squared of the aforementioned components, is ±0.5 K.

The error in the cold reference measurement is caused mainly by the residual error in coupling between the cold sky reflector and the feedhorn. This is estimated to be ±0.5 K. Other factors affecting the cold reference error are the reflections out of the feedhorn due to the receiver electronics, and the resistive losses of the cold sky reflector itself. An estimate of this error can be as high as ±0.62 K.

The main factor influencing radiometer nonlinearity is imperfect operation of the square law detector. This nonlinearity results in an error that can be estimated during the thermal-vacuum calibration testing. (On SSM/I this error was ±0.4 K.) Another source of error in the receiver electronics is the gain drift caused by instrument temperature variation over one orbit. This error

Table 4. AMSR Standard Data Products

Product Level	Parameter	Accuracy	Spatial Resolution (km)
1C	Brightness Temp. (Global), K	0.2 - 0.7 K	6 - 76
2	Wind Speed (Ocean), m s^{-1}	1.5 m s^{-1}	14
2	Precipitable Water (Ocean), g cm^{-2}	0.2 g cm^{-2}	28
2	Cloud Liquid Water, mg cm^{-2} Total Column (Ocean)	3 mg cm^{-2}	28
2	Sea Surface Temperature, K	0.5 K	76
2	Precipitation (Land), mm hr^{-1}	40%	14
2	Precipitation (Ocean), mm hr^{-1}	20%	49
2	Sea Ice Type	11%	14
2	Sea Ice Concentration, %	7%	14
2	Snow Depth, TBD	TBD	31
2	Snow Water Content, TBD (Liquid Water Equivalent)	TBD	31
2	Surface soil moisture, g cm^{-3}	0.06 g cm^{-3}	76
2	Land-surface temperature, °C	2.5 °C	76
2	Vegetation water content, kg m^{-2}		76

depends on the design of the receiver and the overall design of the sensor. The drift can be as high as ±0.24 K for a temperature variation of less than 10 °C over one orbit.

2.3.3 Standard Data Products

For each EOS instrument, there exists a suite of EOS standard data products. Each EOS instrument science team develops, validates, and maintains the alogrithms and science software that produce their instrument's standard data products. EOS defines five levels of EOS standard data products, described in Table 2. Level 1 includes three sublevels—Level 1A, which refers to uncalibrated data (with engineering and ancillary data appended); Level 1B, which refers to radiometrically calibrated data at the original sampling locations; and Level 1C, which refers to calibrated, co-registered, and comensurate data, such that for given subsets of channels, the brightness temperatures of all channels in those subsets represent the same spatial regions on the ground (the effective antenna patterns and sampling locations are the same). The current list of standard data products to be produced by the EOS AMSR Science Team is shown in Table 4. The Level 2 land products provided by this investigation will be generated from the Level 1C product

provided by F. Wentz. It is important that we use this Level 1C product, since the multichannel retrieval algorithm assumes that, at each retrieval point, the 6.9 and 10.6 GHz brightness temperatures are characteristic of the same region of terrain (i.e. they have the same footprint size and location).

3. ALGORITHM DESCRIPTION

3.1 THEORETICAL DESCRIPTION

The retrieval algorithm for m_e, T_e, and w_e is based on a physical radiative-transfer model which relates parameters describing the surface and atmosphere to the observed brightness temperatures. The model is a synthesis of state-of-the-art knowledge of microwave emission and transfer through soils, vegetation, and the atmosphere. The model represents these processes in simplified form, but as realistically as possible at the spatial scales appropriate to the AMSR footprints. The parameterization of the forward model is designed with the inverse retrieval algorithm in mind. Errors in model-approximations of the true physics, and a-priori uncertainties in the model parameters, will be reflected in the resulting retrieval errors. These model errors and uncertainties have been estimated as quantitatively as possible, and their influences on retrieval error have been evaluated by a sensitivity analysis. Soil surface roughness and vegetation scattering are difficult to model accurately at frequencies above 37 GHz, and limited experimental measurements of soils and vegetation have been performed above this frequency. Hence, our physically-based retrieval algorithm uses only the lower AMSR frequencies (6.9 and 10.7 GHz). The 37 and 89 GHz channels of AMSR will be used as qualitative indices only, for long-term monitoring and quality control.

3.1.1 Physics of the Problem

(a) Emission from bare soils

For a homogeneous soil with smooth surface, the reflectivities at vertical and horizontal polarizations, r_{o_v} and r_{o_h}, are given by the Fresnel expressions:

$$r_{o_v} = \left| \frac{\varepsilon_r \cos\theta - \sqrt{\varepsilon_r - \sin^2\theta}}{\varepsilon_r \cos\theta + \sqrt{\varepsilon_r - \sin^2\theta}} \right|^2 \tag{1}$$

$$r_{o_h} = \left| \frac{\cos\theta - \sqrt{\varepsilon_r - \sin^2\theta}}{\cos\theta + \sqrt{\varepsilon_r - \sin^2\theta}} \right|^2 \tag{2}$$

where θ is the incidence angle (relative to the surface normal), and ε_r is the complex dielectric constant of the soil. For a given frequency, the dielectric constant depends primarily on the volumetric soil moisture content, m, and to a lesser extent on soil type. There is also a slight dependence on soil temperature. The soil can be considered as a component mixture of soil particles and pore spaces filled with air and water (Wang and Schmugge, 1980; Dobson et al.,

1985). The model used in this investigation to relate dielectric constant to soil moisture is that of Dobson et al (1985) The dielectric model requires the specification of the sand and clay mass fractions, s and c, (which describe the soil texture) and the soil bulk density, ρ_b. The smooth-surface emissivity, e_{o_p}, is related to the reflectivity, r_{o_p}, by reciprocity:

$$e_{o_p} = 1 - r_{o_p} \tag{3}$$

where the subscript p denotes either vertical or horizontal polarization ($p = v$ or h). Figure 4 shows experimental observations of emissivity as a function of soil moisture at 1.4 GHz, for bare, smooth soils. Also shown are the theoretical curves derived from the two dielectric models mentioned above. The high sensitivity of brightness temperature to soil moisture, ~3 K/% volumetric soil moisture (for a soil temperature of 300 K), is the primary driver for the use of microwave radiometry for soil moisture sensing.

For a soil of uniform temperature, T_s, the soil brightness temperature, T_{bs_p}, is given by

$$T_{bs_p} = e_{o_p} T_s \tag{4}$$

Under natural conditions, the soil temperature has a nonuniform, time-varying, vertical profile determined by the net heat-flux at the surface and the soil thermal properties. The moisture profile is also nonuniform and time-varying, driven primarily by the net moisture flux at the surface (precipitation minus evaporation), and dependent on the hydraulic properties of the soil. The temperature- and moisture-profile dynamics are coupled, since the thermal properties depend on the moisture. For a soil of homogeneous characteristics (i.e. thermal and hydraulic properties), the space-time dynamics of the temperature and soil profiles can be described straightforwardly using one-dimensional equations of coupled moisture- and heat-flux since temperature and moisture vary in the vertical dimension only. For heterogeneous soils, such modeling is difficult since the spatial variability extends to three dimensions and the heterogeneity is difficult to parameterize for modeling purposes. Fortunately, for the microwave retrieval algorithm, we do not need to model the dynamics of the soil profiles—we need only to understand the extent of typical profile variability encountered in nature and to model the effects of such variability on the emitted brightness. To the extent that the soil heat- and moisture-flux models provide time-dependent information and constraints on the variability of the moisture and temperature profiles, these models and information can be incorporated beneficially into the retrieval algorithms to provide improved soil moisture and temperature estimates.

For nonuniform temperature and moisture profiles, the dependence of the soil brightness temperature, T_{bs_p}, on subsurface variability of temperature, $T_s(z)$, and moisture, $m(z)$, can be expressed as:

$$T_{bs_p} = \int_{-\infty}^{0} T_s(z)\, F_p\{\varepsilon_r(z)\}\, dz \tag{5}$$

where z is the vertical dimension (positive in the upward direction). The form of $F_p\{\varepsilon_r(z)\}$ can be determined using models of coherent electromagnetic propagation in a continuous or stratified medium (Njoku and Kong, 1977).

Approximate Form: An approximate form for $F_p\{\varepsilon_r(z)\}$, valid when the moisture profile does not vary rapidly over the depth of a wavelength in the medium (the wavelength in the medium varies with dielectric constant and hence also with depth), can be determined using an incoherent radiative transfer approach, which leads to expressions equivalent to (5):

$$T_{bs_p} = (1 - r_{o_p})\, T_{se} \tag{6}$$

$$T_{se} = \int_{-\infty}^{0} T_s(z)\, \widetilde{F}_{N_p}\{\varepsilon_r(z)\}\, dz \tag{7}$$

where r_{o_p} now denotes the Fresnel reflectivity of a homogeneous soil of dielectric constant $\varepsilon_r(0)$, (i.e. $\varepsilon_r(z)$ at z = 0), T_{se} is the soil "effective temperature", and $\widetilde{F}_{N_p}\{\varepsilon_r(z)\}$ is an approximation of $F_p\{\varepsilon_r(z)\}$, normalized to an integral of unity:

$$\widetilde{F}_{N_p}\{\varepsilon_r(z)\} = \alpha(z) \exp\left(-\int_{z}^{0} \alpha(z')\, dz'\right) \tag{8}$$

$$\alpha(z) = 2\, Im\left\{\frac{2\pi}{\lambda}\sqrt{\varepsilon_r(z) - \sin^2\theta}\right\} \tag{9}$$

Equations (6)-(9) can be derived directly as a first-order approximation to Equation (5) (Njoku and Kong, 1977). They express the fact that, to first order, the reflectivity (and emissivity) of a soil is determined by the dielectric constant (and hence the soil moisture) at the soil surface ($z = 0$), while the brightness temperature is affected by the subsurface temperature and moisture profiles. This approximation is convenient, since Equation (6) has a simple form equivalent to Equation (4). As the wavelength increases, the approximation becomes less accurate, as the emissivity becomes dependent not just on the surface dielectric constant but on the subsurface gradient of the dielectric constant also. However, the approximation is still useful, provided that the emissivity is considered to be representative of the *average* moisture within a top soil layer of depth d_m, the "moisture sensing depth", where d_m depends on wavelength. Simulations have shown (Wilheit, 1978), that d_m is about a tenth of a wavelength in the medium. Thus, d_m is a variable that is dependent on the surface soil moisture content. The longest AMSR wavelength is 4.3 cm, and for a dry soil the wavelength in the medium will be about half this value. Thus, we find for AMSR that $d_m < 2$ mm. The AMSR soil moisture retrieval is therefore very much a "skin surface" value.

The approximation becomes invalid at longer wavelengths if there are sharp moisture profile discontinuities close to the surface, such as for a rapidly drying surface or sharp wetting front, or a shallow water table. Although these occurences do not comprise a significant percentage of natural conditions, such conditions may cause anomalous retrievals.

Weighting Functions: Figure 5 shows the weighting functions, $\widetilde{F}_{N_p}\{\varepsilon_r(z)\}$, for two representative moisture profiles. The bulk of the soil emission comes from the neighborhood around the maxima of the weighting functions, which may occur significantly below the surface for some profiles. For uniform soil moisture (i.e. uniform dielectric constant), and nadir-viewing, $\widetilde{F}_{N_p}\{\varepsilon_r(z)\}$ takes the simple form:

$$\widetilde{F}_{N_p}\{\varepsilon_r(z)\} = \alpha \exp(\alpha z) \tag{10}$$

$$\alpha = \frac{4\pi n''}{\lambda} \tag{11}$$

where n'' is the imaginary part of the refractive index (square root of the dielectric constant), i.e. $n'' = Im\{\sqrt{\varepsilon_r}\}$. The "temperature sensing depth", $d_t = \alpha^{-1}$, is defined as the depth of the surface layer from which ~63% of the emitted radiation originates. From an alternate perspective, d_t is the distance in the medium over which the intensity of transmitted radiation decreases by a factor of $e^{-1} = 0.368$ (for a medium of uniform temperature and moisture). d_t is also commonly referred to as the "penetration depth" in the medium. In summary, the moisture and temperature sensing depths, d_m and d_t, define the approximate depths within which the soil moisture influences emissivity, and the soil moisture and temperature together influence effective temperature, respectively. These parameters are useful in describing the characteristics of microwave emission from soils. Figure 6 shows the dependence of d_t on frequency and soil moisture for a sandy soil.

Rough Surface: The expressions for reflectivity (Equations (1) and (2)) must be modified for rough surfaces, to take into account the effects of surface scattering. The reflectivity of a rough soil, r_{s_p}, can be expressed as (Peake, 1959):

$$r_{s_p}(\theta, \phi) = \frac{1}{4\pi} \int \int_{2\pi} \left[\gamma_{pp}(\theta, \phi;\ \theta', \phi') + \gamma_{pq}(\theta, \phi;\ \theta', \phi')\right] d\Omega' \tag{12}$$

in which the polarizations (p, q) refer to (h, v), or vice versa, and γ_{pp} and γ_{pq} are the co- and cross-polarized bistatic scattering coefficients for radiation scattered from an incident direction (θ, ϕ) into a scattered direction (θ', ϕ'). The solid angle integration is taken over the upper hemisphere. The bistatic coefficients are equivalent to the radar backscattering coefficients when $(\theta, \phi) = (\theta', \phi')$. In practice it is difficult to compute the reflectivity using Equation (12) since this requires deriving expressions for the scattering coefficients and performing a two-dimensional integral. The scattering coefficients can be computed by assuming either a deterministic form or a statistical distribution function for the surface roughness, such as periodic, as with a furrowed field, or randomly rough, as is more often the case in natural environments. Randomly rough surfaces may be modeled statistically in terms of two parameters: the height standard deviation, σ, and the horizontal correlation length, l. Many approaches to deriving theoretical expressions for reflectivity have been developed using these parameters (e.g. Fung and Eom, 1981; Tsang and Newton, 1982; Tsang et al., 1985). Although they provide insight into the scattering mechanisms, these expressions are not easy to use since they require detailed knowledge of the soil surface height and slope statistics, and their computational accuracy is often limited in practical situations.

A simpler, semi-empirical formulation has been proposed (Wang and Choudhury, 1981; Wang et al., 1983) which also includes two surface parameters: a height parameter, h (which is related to σ), and a polarization mixing parameter, Q (which is related to both σ and l). The reflectivity, r_{s_p}, is then related to that of a smooth soil, r_{o_p}, by:

$$r_{s_v} = [\,(1 - Q)\, r_{o_v} + Q\, r_{o_h}\,] \exp(-h) \tag{13}$$

$$r_{s_h} = [\,(1 - Q)\, r_{o_h} + Q\, r_{o_v}\,]\, exp(-h) \tag{14}$$

Values for Q and h' have been determined for some soil roughness conditions from ground-based radiometer observations. However the experimental database is currently too limited to validate quantitatively these roughness parameterizations over a substantial range of conditions. For analysis of data at 1.4 GHz, when surface roughness conditions may be unknown, a value of zero is often assigned to Q, and a value between 0 and 0.3 is typically assumed for h (Jackson, 1993). It must be emphasized that the above modeling descriptions do not attempt to fully describe or represent the detailed scales of roughness variability present in nature, i.e. specific geometric structures, azimuthal anisotropy, time-varying (wind-generated) roughness, etc., but only to capture in simplified form, and with few parameters, the major phenomenological and observable roughness effects on microwave brightness. In the retrieval algorithm developed here, the parameters h and Q are considered as "calibration parameters". They will be estimated empirically, and for a given location are not expected to vary significantly over time at the ~70-km AMSR scale.

(b) Vegetation Effects

Vegetation is represented in the model as a uniform, single-scattering layer above a rough soil. The subsurface soil parameters (moisture and temperature) may vary with depth. However, the soil characteristics—texture, hydraulic, and thermal properties, etc.—are considered uniform with depth. Following the treatments of Mo et al. (1982) and Kerr and Njoku (1990) the brightness temperature at the top of the vegetation layer, T_{b_p}, can be written as a function of soil brightness temperature, T_{bs_p}, soil reflectivity, r_{s_p}, vegetation opacity, τ_c, vegetation single-scattering albedo, ω_p, and vegetation effective temperature, T_{ce}:

$$T_{b_p} = T_{bs_p} \exp(-\tau_c) + T_{ce}\,(1 - \omega_p)\,[1 - \exp(-\tau_c)]\,[1 + r_{s_p} \exp(-\tau_c)] \tag{15}$$

The reflectivity of the two-layer soil/vegetation surface, r_p, is a function of the soil reflectivity, r_{s_p}, and vegetation opacity, τ_c:

$$r_p = r_{s_p}\, exp(-2\tau_c) \tag{16}$$

Use of the term "effective temperature" for the soil and vegetation temperatures in Equations (7) and (15) emphasizes the fact that when the physical temperatures of the media are nonuniform the effective temperatures appearing in the radiative transfer expressions are weighted means of the actual temperatures. (In the model used here the vegetation temperature is considered uniform, hence in this case T_{ce} is the actual vegetation temperature.) In Equation (15) the single scattering albedo has a polarization dependence since the scattering depends on the relative orientations of

leaves, stalks, and branches within the vegetation volume (Karam et al., 1992). The opacity, τ_c, may also exhibit a polarization dependence, but there is little evidence to show that this is of comparable significance to the other modeled effects.

The dependence of τ_c on vegetation columnar water content, W_c, follows an approximately linear relationship which may be written as:

$$\tau_c = b\, W_c / \cos\theta \tag{17}$$

The factor, $\cos\theta$, accounts for the slant observation path through the vegetation, and b is a parameter that depends weakly on vegetation type at low frequencies (< 10 to 15 GHz), and is approximately proportional to frequency in this range (Jackson and Schmugge, 1991) The single-scattering albedo, ω_p, does not exhibit a significant, observable dependence on frequency or vegetation water content. It is also considered a calibration parameter in the retrieval algorithm.

(c) Surface Heterogeneity

For a heterogeneous scene (Figure 7), Equation (15) must be interpreted in the sense that the parameters and terms represent area-weighted averages over the scene components within the observed footprint. The horizontal footprint dimension and area-weighting are defined by the antenna pattern, which can be viewed as a two-dimensional weighting function.

If we consider a simple representation, in which the antenna pattern is constant within the footprint area, and zero outside, then the observed brightness temperature, T_b, will be an area-average of the component brightness temperatures, T_{b_j}, within the footprint, i.e.

$$T_b = \sum_{j=1}^{N} f_j\, T_{b_j} \tag{18}$$

where f_j are the fractional coverages of N distinct surface types within the footprint (the f_j sum to unity). A simplified analysis carried out by Njoku et al. (1995b) shows that estimates of area-averaged geophysical variables (surface temperature, T_e, vegetation water content, W_c, and soil moisture, m) retrieved from the area-averaged brightnesses, T_b,will be related to the component variables by the following equations:

$$T_e = \frac{1}{e} \sum_{j=1}^{N} f_j\, e_j\, T_{e_j} \tag{19}$$

$$W_c = -\frac{\cos\theta}{b}\, ln \left\{ \sum_{j=1}^{N} f_j\, exp[-b\, W_{c_j}/cos\theta] \right\} \tag{20}$$

$$m = \frac{\sum_{j=1}^{N} f_j\, m_j\, exp[-b\, W_{c_j}/cos\theta]}{exp[-b\, W_c/cos\theta]} \tag{21}$$

$$e = \sum_{j=1}^{N} f_j e_j \tag{22}$$

The effects of nonlinearity caused by the presence of vegetation are evident. We may define "composite" parameters, x', (where x may refer to T_e, W_c, or m) as those obtained by a straight area-averaging of the geophysical variables over the footprint, i.e.

$$x' = \sum_{j=1}^{N} f_j \; x_j \tag{23}$$

We can then examine the differences, $\Delta x = x - x'$, between variables retrieved from area-averaged brightnesses (Equations (20)-(22)) and those obtained directly by area-averaging the component variables (Equation (23)). Simulations of Δx have been carried out for a variety of two-component surfaces (Njoku et al., 1995b). Figure 8 shows the results for soil moisture, Δm. The effects of nonlinearity are not large, except in situations of large contrasts within the footprint between roughly equal fractions of bare soil and dense vegetation. These cases will be considered carefully when interpreting the AMSR land retrievals.

For purpose of our simplified model description, we limit further treatment here to the two-component case of uniform vegetation and bare soil, which considers, satisfactorily, the most significant effects of heterogeneity. In this case, $N = 2$, and we can denote f_1 as the vegetation fractional cover, and $f_2 = 1 - f_1$ as the bare-soil fractional cover. The bare-soil brightness temperature, $T_{b_{p2}}$, for scene component $j = 2$, is computed from Equation (6) (with r_{o_p} replaced by the rough soil form, r_{s_p} (Equations (13) and (14)). The vegetated-surface brightness temperature, $T_{b_{p1}}$, for scene component $j = 1$, is computed from Equation (15), with the additional simplification that the soil underneath the vegetation layer is considered to be at the same temperature as the vegetation, i.e. $T_{se} = T_{ce}$ (for this fraction of the scene only).

(d) Atmospheric Effects

The microwave brightness temperature, T_{B_p}, observed by a spaceborne radiometer above the atmosphere is given by:

$$T_{B_p} = T_u + \exp(-\tau_a)\,[T_{b_p} + r_p\,\{T_d + T_{sky}\exp(-\tau_a)\}] \tag{24}$$

where T_u and T_d are the upwelling and downwelling atmospheric radiation, T_{sky} is the space background brightness (2.7 K), τ_a is the atmospheric opacity, r_p is the surface reflectivity, and T_{b_p} is the surface brightness temperature (Equations (15) and (16)). Standard radiative transfer expressions for T_u and T_d may be found in the literature, e.g. Hofer and Njoku (1981). For low atmospheric absorption (as is the case at 6.9 and 10.6 GHz), T_u and T_d can be expressed using the effective radiating temperature approximation:

$$T_u \cong T_d \cong T_{ae}\,[1 - \exp(-\tau_a)] \tag{25}$$

where, T_{ae} is the weighted-mean temperature of the microwave-absorbing region of the atmosphere. This expression is accurate at f < 11 GHz over a wide range of atmospheric temperature and water vapor profiles and cloud conditions. T_{ae} is frequency dependent, and depends also on the vertical distributions of atmospheric temperature, humidity, and liquid water. For f < 11 GHz, the dependence of T_{ae} on atmospheric profile variability is small, and T_{ae} may be expressed simply as a function of the surface air temperature, T_{as}, and a frequency-dependent offset δT_a:

$$T_{ae} \cong T_{as} - \delta T_a \tag{26}$$

Values for δT_a are obtained from calculations using climatological atmospheric data, neglecting effects of clouds and rain.

The opacity, τ_a, along the slant-range atmospheric path is dependent on the viewing angle, θ, and the vertical-column amounts of water vapor, l_v, and cloud liquid water, l_w, in the atmosphere, and can be written (for a plane parallel atmosphere) as:

$$\tau_a = (a_o + a_v\, l_v + a_w\, l_w) / \cos\theta \tag{27}$$

where, a_o, a_v, and a_w are frequency-dependent coefficients.

(e) Model Summary, $T_{B_i} = \Phi_i(\mathbf{x})$

The soil-vegetation-atmosphere radiative transfer model described by Equations (1), (2), (6), (13)–(17), and (24)–(27) can be represented as:

$$T_{B_i} = \Phi_i(\mathbf{x}) \tag{28}$$

where the model function, $\Phi_i(\mathbf{x})$, relates brightness temperature observations, T_{B_i}, at channel i, to the parameters, $\mathbf{x} = \{x_j\}$, of the soil-vegetation-atmosphere medium.

The model parameters are listed in Table 5. The parameters are grouped in two categories: (a) parameters defining sensor and media characteristics or empirical relationships, and (b) retrievable geophysical variables. The atmospheric variables are included in the retrievable list although the sensitivity of brightness temperature to these variables (over land), at frequencies below 37 GHz, is too low to afford reliable retrieval accuracies. (Retrieval of water vapor may be possible over some surfaces of low variability, particularly if ancillary data are available to characterize the background surface.

Table 5: Parameters of the Microwave Model, $\Phi_i(\mathbf{x})$

Parameters	Description
(a) Media/Sensor Parameters	
Atmosphere:	
a_o	Oxygen opacity
a_v, a_w	Water vapor and liquid opacity coefficients
δT_a	Absorption-temperature differential, K
Vegetation:	
ω_p	Single scattering albedo
b	Opacity coefficient
f_1	Fractional cover
Soil:	
h, Q	Roughness coefficients
ρ_b	Bulk density, g cm^{-3}
s, c	Sand and clay mass fractions
Sensor:	
θ	Viewing angle, deg
ν	Frequency, GHz
p	Polarization
(b) Media Variables	
Atmosphere:	
l_v	Columnar water vapor, g cm^{-2}
l_w	Columnar liquid water,
T_{as}	Surface air temperature, K
Vegetation:	
T_{ce}	Effective temperature, K
W_c	Water content, kg m^{-2}
Soil:	
m	Surface moisture content, g cm^{-3}
T_{se}	Effective Temperature, K

(e) Sensitivities

The normalized sensitivity, S_i, of brightness temperature to a given geophysical parameter, x_i, can be expressed as:

$$S_i = \left| X_i \left(\frac{\partial \Phi}{\partial x_i} \right)_{\mathbf{x} = \mathbf{x}_o} \right| \tag{29}$$

where X_i are typical geophysical parameter dynamic ranges, and $\mathbf{x}_o$ are baseline values of the parameters, $\mathbf{x}$, at which the sensitivities are evaluated. Normalized sensitivities are computed to indicate more realistically the relative magnitudes of the sensitivities to the different geophysical variables, in Kelvins. Table 6 shows the computed sensitivities, for horizontal and vertical polarizations, at 6.9 GHz. Two cases are shown, one for a baseline of bare soil and one for vegetation water content of 1.5 kg m^{-2} (spanning the range of vegetation conditions under which we believe soil moisture retrievals will be feasible). The sensitivity to moisture and vegetation are clearly much reduced for the higher vegetation level, although good sensitivity remains to surface temperature. The sensitivity differences between H and V polarizations, and between frequencies (10.6 GHz not shown), enable the four-channel retrieval algorithm to discriminate satisfactorily between the moisture, vegetation, and temperature variables. Sensitivities to other variable and model parameters are typically an order of magnitude or so less than to the three main variables (soil moisture, surface temperature, and vegetation water content), and hence are not dominant factors in the retrievals.

Table 6(a): Normalized sensitivities at 6.6 GHz H and V polarizations, θ = 50°, for given parameter ranges, X_i, and baseline values, x_{oi}. Vegetation baseline = 0 kg m^{-2} (bare soil).

Parameter	Range (X_i)	Baseline (x_{oi})	Sensitivity, H S_i (K)	Sensitivity, V S_i (K)
Soil moisture (g cm^{-3})	0.32	0.15	95.5	60.1
Surface temperature (°C)	40	20	25.1	35.7
Vegetation water (kg m^{-2})	1.5	0	211.3	28.1
Atmos. Water Vapor (mm)	5	2.5	1.3	0.18

Table 6(b): As for Table 6(a), except vegetation baseline = 1.5 kg m^{-2}.

Parameter	Range (X_i)	Baseline (x_{oi})	Sensitivity, H S_i (K)	Sensitivity, V S_i (K)
Soil moisture (g cm^{-3})	0.32	0.15	8.5	5.3
Surface temperature (°C)	40	20	22.0	20.6
Vegetation water (kg m^{-2})	1.5	1.5	10.9	1.2
Atmos. Water Vapor (mm)	5	2.5	0.12	0.02

(f) Retrieval Model Approximation, $T_{B_i}' = \Phi_i'(\mathbf{x})$

In order to reduce the parameterization of the microwave model to a convenient set of three dominant surface variables that can be retrieved from the four low-frequency AMSR channels, the following approximations are made:

(1) The soil moisture profile is considered uniform.

(2) The soil and vegetation temperature profiles are considered uniform.

(3) The surface is considered uniformly-vegetated, i.e. $f_1 = 1$. All retrieved parameters, m_e, T_e, and w_e, will then represent area-averaged quantities over the ~ 70-km AMSR footprint.

With these approximations, we distinguish this simplified model from that above by using the notation:

$$T_{B_i}' = \Phi_i'(\mathbf{x}) \tag{30}$$

The three retrievable variables are then:

- m_e : Surface soil moisture (g cm^{-3})—the area-averaged mean moisture in the top few mm (skin surface layer) of soil.
- w_e : Vegetation water content (kg m^{-2})—the area-averaged water content in the vertical column of vegetation overlying the soil.
- T_e : Land-surface temperature (K)—the area-averaged mean 6.9 and 10.7 GHz microwave radiating temperature of the surface.

A nonlinear parameter estimation method is used as the baseline algorithm for deriving the AMSR land-surface parameters. The algorithm is based on the radiative transfer model, $\Phi_i'(\mathbf{x})$.

3.1.2 Mathematical Description of the Algorithm

Passive microwave retrievals of land surface parameters have in the past used mainly surface classification and linear-regression methods (e.g. Jackson and LeVine, 1996). Nonlinear algorithms (iterative and neural-network based) have also been used, particularly to improve retrievals where the physics of the radiative transfer and interaction processes are nonlinear (Zurk et al., 1992; Njoku et al., 1994). Bayesian estimation techniques have also been investigated to include, optimally, a-priori information on sensor noise, model uncertainties, probability distributions of the parameters being estimated, and ancillary data from ground truth or other sensors. (Davis et al., 1995).

(a) Baseline Algorithm

The baseline AMSR land-surface-products computational procedure uses a nonlinear, iterative retrieval algorithm to simultaneously retrieve the three primary variables, m_e, w_e, and T_e, from measurements at four channels (i = 1 to 4). The procedure adjusts the set of variables $\mathbf{x} = \{m_e, w_e, \text{ and } T_e\}$ so as to minimize the weighted-sum of squared differences, χ^2, between observed, $T_{B_i}^{obs}$, and computed, $\Phi_i'(\mathbf{x})$, brightness temperatures. The efficient Levenberg-Marquardt minimization algorithm is used (Press et al., 1989).

$$\chi^2 = \sum_{i=1}^{4} \left(\frac{T_{B_i}^{obs} - \Phi_i'(\mathbf{x})}{\sigma_i} \right)^2 \tag{31}$$

At each retrieval point, the algorithm starts with a-priori values of the geophysical variables, $\mathbf{x_o}$, and adjusts these iteratively until convergence to the χ^2 minimum is achieved. σ_i represents the measurement noise in channel i. Since the forward model, $\Phi'_i(\mathbf{x})$, is mathematically well-behaved, convergence is rapid and accurate, except where the forward model does not adequately represent the large-area emission physics (e.g. where snow or open water occur in the footprint), or where the sensitivity to a given parameter is too low. This occurs, for example, in the retrieval of m_e and w_e in densely-vegetated areas. In these cases the retrieved values of m_e and w_e will be meaningless. In actual operation of the algorithm, the m_e and w_e retrieval errors increase as a function of increasing vegetation content. Atmospheric variables of the model—l_v, l_w, T_{as}, and δT_a—are given a-priori values derived from climatologies and/or model output (Meeson et al., 1995; Bengtsson et al., 1982). The atmospheric parameters a_o, a_v, and a_w, are constants, and are well-known from the literature. The parameters b, h, Q, ω_p, ρ_b, s, and c are given fixed values, which may require empirical fine-tuning in the immediate post-launch period, to compensate for residual uncertainties and offsets in the physical model and to "calibrate" the model to AMSR observations at designated calibration sites.

(b) Enhanced Algorithm

An algorithm based on Bayesian estimation, as described by Davis et al. (1995), will be investigated in a research mode for implementing constraints on the retrievals in a formal way—by incorporating a-priori statistics (probability distributions) of the surface and atmospheric

characteristics. Such information will be obtained from vegetation and soils data (Wilson and Henderson-Sellers, 1985), digital topographic data at scales comparable to the satellite footprint (U.S. Geological Survey), operational ECMWF surface air temperature and humidity fields (Bengtsson et al., 1982), and other model output and climatological fields (Meeson et al., 1995). Much of the flexibility in the Bayesian approach lies in the ability to adjust the a-priori distribution covariances relative to the sensor and model mismatch covariances in order to ensure stable and well-behaved retrievals. The a-priori geophysical variable covariances will be poorly known at the start of the AMSR mission. However, as the database of global retrievals is built up after launch, the algorithm will actually "learn" and become more optimal in the sense of utilizing improved a-priori knowledge of the geophysical variables.

(c) Output products

Global retrieved-variable data sets will be generated in swath format (level 2). Level 3 products will be generated from level 2 in order to analyze global gridded fields and to develop higher level products. The level 3 products will include day minus night brightness temperature and surface temperature difference products, to investigate the use of diurnal variability in obtaining additional soil moisture information, and for use with climate models (Randall et al., 1991; Pitman and Henderson-Sellers, 1995). Level 2 products will be produced at the original sampling and spatial resolution of the level 1C input data. Level 3 products will be produced on a 0.25° x 0.25° latitude-longitude grid. Consideration will be given to producing the data on other grids (such as the NSIDC EASE-Grid). Output data will include quality flags indicating the expected accuracy of the retrievals at each point.

3.1.3 Variance and Uncertainty Estimates

Monte Carlo simulations are currently being performed to estimate the retrieval uncertainties of the baseline algorithm. Parameters of the forward model are assigned probability distributions with variances representative of their a-priori uncertainties. The variables to be estimated, $\mathbf{x} = \{m_e, w_e, T_e\}$, are simulated as sets of uniform random variates spanning the dynamic ranges: m_e = 0.03 to 0.35 g cm^{-3}; w_e, = 0 to 5 kg m^{-2}; T_e = 0 to 40 °C. From these parameter and variable distributions, brightness temperatures, $T_{B_i} = \Phi_i(\mathbf{x})$, are computed at the four AMSR channels used in the retrieval (6.9 and 10.6 GHz; V and H polarizations). To these brightness temperatures gaussian random noise of 0.3 K (1σ) is added to simulate the AMSR observations, $T_{B_i}^{obs}*$. The retrieval algorithm is applied to the simulated observations, and parameter estimates, $\mathbf{x}*$, are obtained. The uncertainty estimates in the retrieval procedure are then given by the mean and standard deviation of the errors, $\varepsilon = \mathbf{x}* - \mathbf{x}$.

3.2 PRACTICAL CONSIDERATIONS

3.2.1 Numerical Computation Considerations

The baseline algorithm has been tested by running it on Nimbus-7 SMMR data, using similar channels, i.e. 6.6 and 10.7 GHz, V and H polarizations. At each retrieval point, from 4 to 8

iterations are normally required for convergence to a solution. A solution is considered a simultaneous retrieval of the three variables m_e, w_e, and T_e. On a SUN IPX Workstation, 1600 solution points encompassing a range of bare and vegetated sites take on average about 3 minutes for computation, or about 112 ms per retrieval point. Additional overhead imposed by exception handling (see below) and output quality control may increase the processing time to a maximum of 250 ms per retrieval point. These numbers will be reduced considerably on the higher-capability workstations envisaged for the AMSR post-launch operational processing.

3.2.2 Programming/Procedural Considerations

The baseline algorithm, in its current version, does not require external inputs from any other data source other than climatology. However, algorithm enhancements will most likely be incorporated prior to algorithm delivery, that make use of surface characteristics and model-output data which will be stored for use by the algorithm. The combined size of these databases is estimated to be on the order of 5 to 20 Mbytes. Algorithms will be written in standard FORTRAN-90 with full portability to run on UNIX-based platforms. Data products will be structured and formatted according to EOSDIS guidelines. Coordination will be maintained with the appropriate EOSDIS DAAC in providing documentation, algorithms, and data appropriate for archival and public distribution.

3.2.3 Calibration and Validation

The accuracy of the retrievals will depend to a large extent on the accuracy of the microwave model. Since radiative transfer models are simplified representations of reality, and since radiometers typically exhibit calibration offsets which may vary from channel to channel, calibration of the models to the satellite data is expected to be required. This will be accomplished by the use of calibration regions, homogeneous over large scales, that can be characterized by a small number of parameters. These regions in general will include tropical forests, desert regions, and transects across desert, savanna, dry and humid forest. Surface truth data, including surface air-temperature, humidity, precipitation, surface moisture, and biomass, available from existing and forthcoming experiments in some of these sites, will be used. Values of single scattering albedo over forests, and surface roughness coefficients over deserts, will be estimated in this manner.

(a) Pre-launch

In the pre-launch phase, the parameterization of the microwave model will be tested using data from the SMMR instrument on Nimbus-7. These data exist from late 1978 through mid-1987, and overlap in time with other datasets of model-output surface moisture and temperature, e.g. the NCEP re-analysis (Kalnay et al.) and the GSFC Data Assimilation Office products. Vegetation data are available from the AVHRR NDVI Pathfinder data set. These data sets can be used as surrogate "climatologies" for the parameters m_e, w_e, and T_e with which to compute brightness temperatures from the microwave model for comparison with the SMMR observations. This will provide the basis for calibrating out biases between the model and observations. This will require fine-tuning after the launch of AMSR since the viewing angles, equator-crossing times,

antenna/radiometer characteristics, and spatial resolutions of AMSR are somewhat different from those of the SMMR.

(b) Post-launch

A major validation challenge will be the quantification of the (vegetation-dependent) soil moisture measurement errors. Systematic comparisons will be required between the soil moisture fields provided by AMSR and those available from alternative measurement systems or as model estimates, while giving appropriate recognition to the vegetation cover prevalent at the comparison site. The AMSR land parameter validation activities will be carried out through collaborations with existing research efforts and field programs, augmenting these where necessary for the specific needs of this investigation. The following plans are being developed specifically through collaborations with other EOS and MTPE investigators for a future dedicated soil moisture mission (2001 and beyond time frame) (personal communication: D. Entekhabi (MIT), J. Shuttleworth (U. Arizona), M. vanGenuchten (USDA), and F. Chen NCEP), and will be pursued also as part of the AMSR investigation.

GCIP and GCIP Follow-on: GCIP is currently providing a 5-year documentation of aspects of hydrologic-atmosphere coupling across the U.S., and will leave in place an ongoing observational framework against which soil moisture comparisons can be made. These data include distributed fields of rainfall from gauges and NEXRAD rain-radar systems, runoff, modeled evaporation, analyzed fields of temperature and humidity, and, at certain locations, arrays of sensors to provide direct measurements of soil moisture. Augmentation of these arrays is being planned within a 200x200 km study area in Oklahoma and Kansas as part of the Atmospheric Radiation Measurement (ARM) Project, and could be extended elsewhere in the Mississippi River basin. These arrays will be valuable as direct sources of comparison data for AMSR over selected regions of the U.S., but can serve also to validate model-based soil-moisture estimates for the U.S. as a whole, which will then be compared with AMSR soil-moisture fields. Maps of vegetation cover will be available from USGS and EOS MODIS land-cover data, with which to evaluate independently the soil-moisture comparisons as a function of vegetation cover.

Detailed Validation Site: The principal validation site being considered covers a large portion (about 10^5 km^2) of the Southern U.S. Great Plains, principally in the state of Oklahoma (D. Entekhabi, personal communication). This region has major East-West precipitation gradients which result in a large range of seasonal soil moisture. The vegetation cover also has a significant range. The region includes several major observation networks and research field sites (OK Mesonet, ARM-CART, ARS Micronet). It is also part of the GEWEX-GCIP focus study area. A list of the available data sources is given in Table 1 (D. Entekhabi, personal communication).

TABLE 1: Characteristics and Sources of Observations for Soil Moisture Validation Data Set Development

Physical Parameter	Spatial Resolution	Temporal Frequency	Source
Surface air Micrometeorology	One Station per 10^3 km^2	15 Minutes	Oklahoma Mesonet
Soil Temperature	One Station per 10^3 km^2	15 Minutes	Oklahoma Mesonet
Soil Matric Head	One Station per 10^3 km^2	15 Minutes Capaticance Probes	Oklahoma Mesonet
Area-Average Precipitation	4 km x 4 km	Hourly	NWS ABRFC
Volumetric Soil Moisture	Variable	Episodic along Flight Lines	NWS NOHRSC Aircraft Instrument (Gamma-Radiation)
Vegetation Parameters	10 km x 10 km 30 km x 30 km	Daily Weekly	Passive Microwave Polar Orbiting (DMSP & EOS) & VIS/IR Geostationary Satellites (GOES-8)
Volumetric Soil Moisture	30 km x 30 km	12 Hourly	NCEP NWP Initialization
Soil Temperature	30 km x 30 km	12 Hourly	NCEP NWP Initialization
Near Surface Air Parameters	30 km x 30 km	12 Hourly	NCEP NWP Initialization
Volumetric Soil Moisture	Point	Episodic	Gravimetric Measurements
Volumetric Soil Moisture	0.5 km x 0.5 km	Episodic	Aicraft remote sensing

Through research collaborations, in which this investigator will play a lead role, a gridded soil moisture validation data product containing fused multi-sensor observations will be produced. Overlapping observations, observations at various scales (point and areal averages) and at different temporal frequencies will be merged using a data fusion methodology that forms statistically optimal estimates of the validation data set state variables (soil moisture and soil temperature in the 0 to -5 cm and -5 to -15, and -15 to -25 cm depths on hourly basis and vegetation leaf area index and dry and moist weight; both on 3 km x 3 km gridding). Weights based on the error structure of different sources of observations will be used to form a single estimate of the state variables. The primary aspects of the validation data strategy are:

(1) Spatially gridded and temporally regular estimates of soil moisture and temperature

(2) Choice of region with large dynamic ranges for vegetation and soil hydrothermal regime

(3) Multi-sensor approach utilizing operational and research observing systems

(4) Data fusion framework based on error structure of incoming data sources

(5) Consistent propagation of state estimates using surface water and energy balance

Global-Scale Validation*:* Validation on a global scale is difficult since the only independent sources are products derived from global atmospheric models, calculated using the soil hydrology from the budgets of energy and water at the Earth's surface. Key parameters, such as precipitation and the surface net radiation, depend on the parameterizations used within the models, and their errors are often hard to assess. Forecast centers routinely perform data assimilation experiments with and without specific satellite products. The regional and global output error fields of critical near-surface parameters would then be examined regionally and globally, such as the 2-m temperature and humidity that are measured in-situ, and are closely linked to soil moisture initialization. The forecast errors resulting from using different soil moisture initializations (model or satellite derived for example) would be examined to assess the impact on the forecast accuracy of the satellite derived soil moisture in comparison with the purely model derived product. These studies will be pursued in collaboration with NCEP and ECMWF (J. Shuttleworth, F. Chen, A. Betts, personal communication*)*.

A separate, but related exercise is currently being pursued using Nimbus-7 SMMR-derived products to compare with model out products of surface soil moisture and temperature

3.2.4 Quality Control and Diagnostics

Outputs of the retrieval algorithm include two diagnostic parameters: (1) N - the number of iterations required to reach convergence; (2) χ^2 - the minimum value of chi-squared achieved. Large values of either N or χ^2 are indicators of non-convergence or large errors in the retrievals.

Gridded fields of the retrieved variables, m_e, w_e, and T_e, will be created by binning the data onto weekly 1/2 x 1/2 degree latitude-longitude grids. The number of samples in each bin, n, and the standard deviations, s_d, will be computed along with the means, x_m, for each bin, to create three sets of gridded fields for each variable. The mean fields will be examined for spatial and

temporal coherence in the geophysical-variable estimates; the number fields will be examined for missing data, gaps in coverage, etc.; and the standard deviation fields will allow anomalous retrievals to be easily identified. Quick-look tools for routinely scanning and summarizing statistics of these fields will be developed as part of this investigation. General-purpose tools currently under development by EOSDIS, or available commercially, will be used to the maximum extent possible.

3.2.5 Exception Handling

The main causes for nonconvergence or errors of the algorithm will be footprints containing open water, snow cover, and heavy clouds or precipitation. Simple tests will be made for open water conditions based on threshholds for the differences between V and H polarizations. This will also be used to identify land versus ocean regions. Footprints identified as containing open water will be flagged as such and no geophysical retrievals will be made. The 37 GHz channels will be used for this purpose, in addition to the 6.9 and 10.6 GHz channels, due to their higher spatial resolution. The 37 and 85 GHz channels will be used to identify and flag footprints containing heavy clouds and precipitation which will degrade the accuracy of the retrievals.

Anomalous inputs may be due to bad radiometric data (e.g. spurious noise, radio-frequency interference, calibration errors, etc.), bad locations, and other lower-level processing errors. Checks will be made in the processing algorithms to identify these anomalies and to assign them flags identifying the type of anomaly and impact on the retrievals. The algorithms will be designed to accommodate small data gaps, where the data are flagged as missing or unusable, without need for re-initialization.

4. CONSTRAINTS, LIMITATIONS, AND ASSUMPTIONS

The retrieval of the specified land products will be limited by the assumptions made in the model, and by the physics of the problem. The following are the major limitations of the output products:

- Footprints may contain mixtures of different surface types, e.g. bare soil, vegetation, rivers. Thus, the retrievals of footprint-averaged soil moisture, temperature, and vegetation, must be interpreted with this in mind. The retrievals nominally represent ~ 70-km area-averages. In cases where there is large contrast (heterogeneity) within a footprint, the retrieved quantities may not accurately represent area-averages due to nonlinearity in the radiative transfer processes. (It is assumed that area-averages are the desired output for large-scale hydrology, climate, and ecological models). This is not expected to be a significant issue based on prior simulations.

- The retrieved variables represent averages over a vertical sampling depth in the medium that is intermediate between the sampling depths at the two frequencies, 6.9 and 10.6 GHz. These depths vary with the amount of moisture in the soil and/or vegetation. The different sampling

depths at 6.9 and 10.6 GHz may give rise to some error in the retrievals where the moisture and temperature profiles are highly nonuniform, since each retrieved variable is defined at a single sampling depth.

- As the vegetation cover increases the retrieval errors for m_e and w_e also increase, until at large values of w_e the retrievals become completely unreliable. The vegetation threshholds for reliability of the retrievals are only roughly-defined at this time. Additional simulations prior to launch, and experience with real AMSR data during the post-launch validation phase, will establish these threshholds more precisely.

- Effects of topography, snow cover, clouds, and precipitation, are not explicitly modeled in the retrieval algorithm. Hence, these effects will manifest themselves as errors in the retrievals. Topographic effects will not change with time, and can be accounted for in enhanced versions of the baseline algorithm.

5. REFERENCES

Asrar and Greenstone (Eds.) (1995): *1995 MTPE/EOS Reference Handbook*. EOS Project Science Office, NASA Goddard Space Flight Center, Greenbelt, MD.

Beljaars, A. C. M., P. Viterbo, M. J. Miller, and A. J. Betts (1996): The anomalous rainfall over the United States during July 1993: Sensitivity to land surface parameterization and soil moisture anomalies. *Mon. Wea. Rev., 124,* 362-383.

Bengtsson, L., M. Kanamitsu, P. Kallberg, and S. Uppala (1982): FGGE 4-dimensional data assimilation at ECMWF, *Bull. Am. Met. Soc., 63,* 29-43.

Brubaker, K. L. and D. Entekhabi (1996): Analysis of feedback mechanisms in land-atmosphere interaction. *Water Resour. Res., 32,* 1343-1357.

Calvet, J.-C., J.-P. Wigneron, E. Mougin, Y. H. Kerr, and J. S. Brito (1994): Plant water content and temperature of the Amazon forest from satellite microwave radiometry. *IEEE Trans. Geosci. Rem. Sens., 32,* 397-408.

Choudhury, B. J., C. J. Tucker, R. E. Golus, and W. W. Newcomb (1987): Monitoring vegetation using Nimbus-7 scanning multichannel microwave radiometer's data. *Int. J. Rem. Sens., 8,* 533-538.

Choudhury, B. J. and R. E. Golus (1988): Estimating soil wetness using satellite data. *Int. J. Rem. Sens., 9,* 1251-1257.

Choudhury, B. J., E. R. Major, E. A. Smith, and F. Becker (1992): Atmospheric effects on SMMR and SSM/I 37 GHz polarization difference over the Sahel. *Int. J. Rem. Sens., 13,* 3443-3463.

Davis, D. T., Z. Chen, J.-N. Hwang, L. Tsang, and E. G. Njoku (1995): Solving inverse problems by Bayesian iterative inversion of a forward model with applications to parameter

mapping using SMMR remote sensing data. *IEEE Trans. Geosci. Rem. Sens., 33*, 1182-1193.

Delworth, T. and S. Manabe (1989): The influence of soil wetness on near-surface atmospheric variability. *J. Clim., 2*, 1447-1462.

Dobson, M. C., F. T. Ulaby, M. T. Hallikainen, and M. A. El-Rayes (1985): Microwave dielectric behaviour of wet soil – Part II: Dielectric mixing models. *IEEE Trans. Geosci. Rem. Sens., GE-23*, 35-46.

Entekhabi, D., H. Nakamura, and E. G. Njoku (1994): Solving the inverse problem for soil moisture and temperature profiles by sequential assimilation of multifrequency remotely sensed observations. *IEEE Trans. Geosci. Rem. Sens., 32*, 438-448.

Fung, A. K. and H. J. Eom (1981): Emission from a Rayleigh layer with irregular boundaries. *J. Quant. Spectr. Radiat. Transfer, 26*, 397-409.

Hofer, R. and E. G. Njoku (1981): Regression techniques for oceanographic parameter retrieval using space-borne microwave radiometry. *IEEE Trans. Geosci. Rem. Sens., GE-19*, 178-189.

Jackson, T. J. and T. J. Schmugge (1991): Vegetation effects on the microwave emission from soils. *Rem. Sens. Environ., 36*, 203-212.

Jackson, T. J. (1993): Measuring surface soil moisture using passive microwave remote sensing. *Hydrological Processes, 7*, 139-152.

Jackson, T. J. and D. E. LeVine (1996): Mapping surface soil moisture using an aircraft-based passive microwave instrument: algorithm and example. *J. Hydrology, 184*, 85-99.

Karam, M. A., A. K. Fung, R. H. Lang, and N. S. Chauhan (1992): A microwave scattering model for layered vegetation. *IEEE Trans. Geosci. Rem. Sens., 30*, 767-784.

Kerr, Y. H. and E. G. Njoku (1990): A semiempirical model for interpreting microwave emission from semiarid land surfaces as seen from space. *IEEE Trans. Geosci. Rem. Sens., 28*, 384-393.

Kerr, Y. H. and E. G. Njoku (1993): On the use of passive microwaves at 37 GHz in remote sensing of vegetation. *Int. J. Rem. Sens., 14*, 1931-1943.

Kerr, Y. H. and J. P. Wigneron (1995): Vegetation models and observations - A review. in: *Passive Microwave Remote Sensing of Land-Atmosphere Interactions (B. Choudhury, Y. Kerr, E. Njoku, and P. Pampaloni, Eds.)*, VSP, Utrecht, The Netherlands.

Lhomme, J. P., A. Chehbouni, and B. Monteny (1994): Effective parameters of surface energy balance in heterogeneous landscapes. *Boundary-Layer Meteorol., 71*, 297-309.

LoSeen, D., A. Chehbouni, E. Njoku, and S. Saatchi (1995): A modeling study on the use of passive microwave data for the monitoring of sparsely vegetated land surfaces. *Proc. IEEE Geoscience and Remote Sensing Symposium (IGARSS'95)*, Florence, Italy.

McFarland, M. J., R. L. Miller, and C. M. U. Neale (1990): Land surface temperature derived from the SSM/I passive microwave brightness temperatures. *IEEE Trans. Geosci. Rem. Sens., 28*(5), 839-845.

Meeson, B. W., F. E. Corprew, J. M. McManus, D. M. Myers, J. W. Closs, K.-J. Sun, D. J. Sunday, and P. J. Sellers (1995): *ISLSCP Initiative I|Global data sets for land-atmosphere models, 1987-1988. Volumes 1-5*. Published on CD by NASA (USA_NASA_GDAAC_ ISLSCP_001 - USA_NASA_GDAACISLSCP_005).

Mo, T., B. J. Choudhury, T. J. Schmugge, J. R. Wang, and T. J. Jackson (1982): A model for microwave emission from vegetation covered fields. *J. Geophys. Res., 87*, 11229-11237.

MTPE (1996): *Mission to Planet Earth Science Strategic Enterprise Plan 1996-2002*, National Aeronautics and Space Administration, Washington, DC.

Njoku, E. G. and J. A. Kong (1977): Theory for passive microwave remote sensing of near-surface soil moisture. *J. Geophys. Res., 82*, 3108-3118.

Njoku, E. G. and I. R. Patel (1986): Observations of the seasonal variability of soil moisture and vegetation cover over Africa using satellite microwave radiometry. *Proc. ISLSCP Conference, Rome, Italy, 2-6 December 1985, ESA SP-248*, European Space Agency, Paris, France.

Njoku, E. G., A. Chehbouni, F. Cabot, B. Rague, K. Fleming, and Y. H. Kerr (1994): An approach to estimating surface parameters and fluxes using modeling and multispectral remote sensing. *Proc. IEEE Geoscience and Remote Sensing Symposium (IGARSS'94), Pasadena, California*.

Njoku, E. G. (1995a): Surface temperature estimation over land using satellite microwave radiometry. In: *Passive Microwave Remote Sensing of Land-Atmosphere Interactions (B. J. Choudhury, Y. H. Kerr, E. G. Njoku, and P. Pampaloni, Eds.)*, VSP, Utrecht, The Netherlands.

Njoku, E. G., S. J. Hook, and A. Chehbouni (1995b): Effects of surface heterogeneity on thermal remote sensing of land parameters. in: *Scaling Up In Hydrology Using Remote Sensing (J. Stewart, E. Engman, R. Feddes, and Y. Kerr, Eds.)*, Wiley, New York.

Norman, J. M. and F. Becker (1995): Terminology in thermal infrared remote sensing of natural surfaces. *Rem. Sens. Rev., 12*, 159-173.

Owe, M., A. Chang, and R. E. Golus (1988): Estimating surface soil moisture from satellite microwave measurements and a satellite-derived vegetation index. *Rem. Sens. Environ., 24*, 131-345.

Owe, M. and A. A. van de Griend (1990): Daily surface moisture model for large area semi-arid land application with limited climate data. *J. Hydrology, 121*, 119-132.

Owe, M., A. A. van de Griend, and A. T. C. Chang (1992): Surface moisture and satellite microwave observations in semiarid southern Africa. *Water Resources Res., 28*, 829-839.

Pitman, A. J. and A. Henderson-Sellers (1996): Simulating the diurnal temperature range: results from Phase 1(a) of the Project for Intercomparison of Landsurface Parameterization Schemes (PILPS), *Atmospheric Research* (in press).

Press, W. H., B. P. Flannery, S. A. Teukolsky, and W. T. Vetterling (1989): *Numerical Recipes* (Ch. 14), Cambridge University Press, New York.

Randall, D. A., Harshvardhan, and D. A. Dazlich (1991): Diurnal variability of the hydrologic cycle in a general circulation model. *J. Atmos. Sci., 48*, 40-62.

Raupach, M. R. and J. J. Finnigan (1995): Scale issues in boundary-layer meteorology: surface energy balances in heterogeneous terrain. *Hydrol. Processes, 9*, 589-612.

Shukla, J. and Y. Mintz (1982): Influence of land-surface evapotranspiration on the Earth's climate. *Science, 215*, 1498-1500.

Sippel, S. J., S. K. Hamilton, J. M. Melack, and B. J. Choudhury (1994): Determination of inundation area in the Amazon river floodplain using the SMMR 37 GHz polarization difference. *Rem. Sens. Environ., 48*, 70-76.

Townshend, J. R. G., C. O. Justice, B. J. Choudhury, C. J. Tucker, V. T. Kalb, and T. E. Goff (1989): A comparison of SMMR and AVHRR data for continental land cover characterization. *Int. J. Rem. Sens., 10*, 1633-1642.

Tsang, L. and R. W. Newton (1982): Microwave emission from soils with rough surfaces. *J. Geophys. Res., 87*, 9017-9024.

Tsang, L., J. A. Kong, and R. T. Shin (1985): *Theory of Microwave Remote Sensing*. J. Wiley and Sons, New York.

van de Griend, A. A. and M. Owe (1994): Microwave vegetation optical depth and inverse modelling of soil emissivity using Nimbus/SMMR satellite observations. *Meteorol. Atmos. Phys., 54*, 225-239.

Wang, J. R. and T. J. Schmugge (1980): An empirical model for the complex dielectric permittivity of soil as a function of water content. *IEEE Trans. Geosci. Rem. Sens., GE-18*, 288-295.

Wang, J. R. and B. J. Choudhury (1981): Remote sening of soil moisture content over bare field at 1.4 GHz frequency. *J. Geophys. Res., 86*, 5277-5282.

Wang, J. R. (1985): Effect of vegetation on soil moisture sensing observed from orbiting microwave radiometers. *Rem. Sens. Environ., 17*, 141-151.

Wei, M.-Y. (1995): *Soil moisture: Report of a workshop held in Tiburon, CA, 25-27 January 1994*. NASA Conference Publication 3319, National Aeronautics and Space Administration, Washington, DC.

Wilheit, T. T. (1978): Radiative transfer in a plane stratified dielectric. *IEEE Trans. Geosci. Rem. Sens., GE-16*, 138-143.

Wilson, M. F. and A. Henderson-Sellers (1985): A global archive of land cover and soil data for use in general circulation climate models, *J. Climatol., 5*, 119-143.

Zurk, L., D. T. Davis, E. G. Njoku, L. Tsang, and J. N. Hwang (1992): Inversion of parameters for semiarid regions by a neural network. *Proc. IEEE Geoscience and Remote Sensing Symposium (IGARSS'92), 1075-1077, Houston, TX, May 1992*.

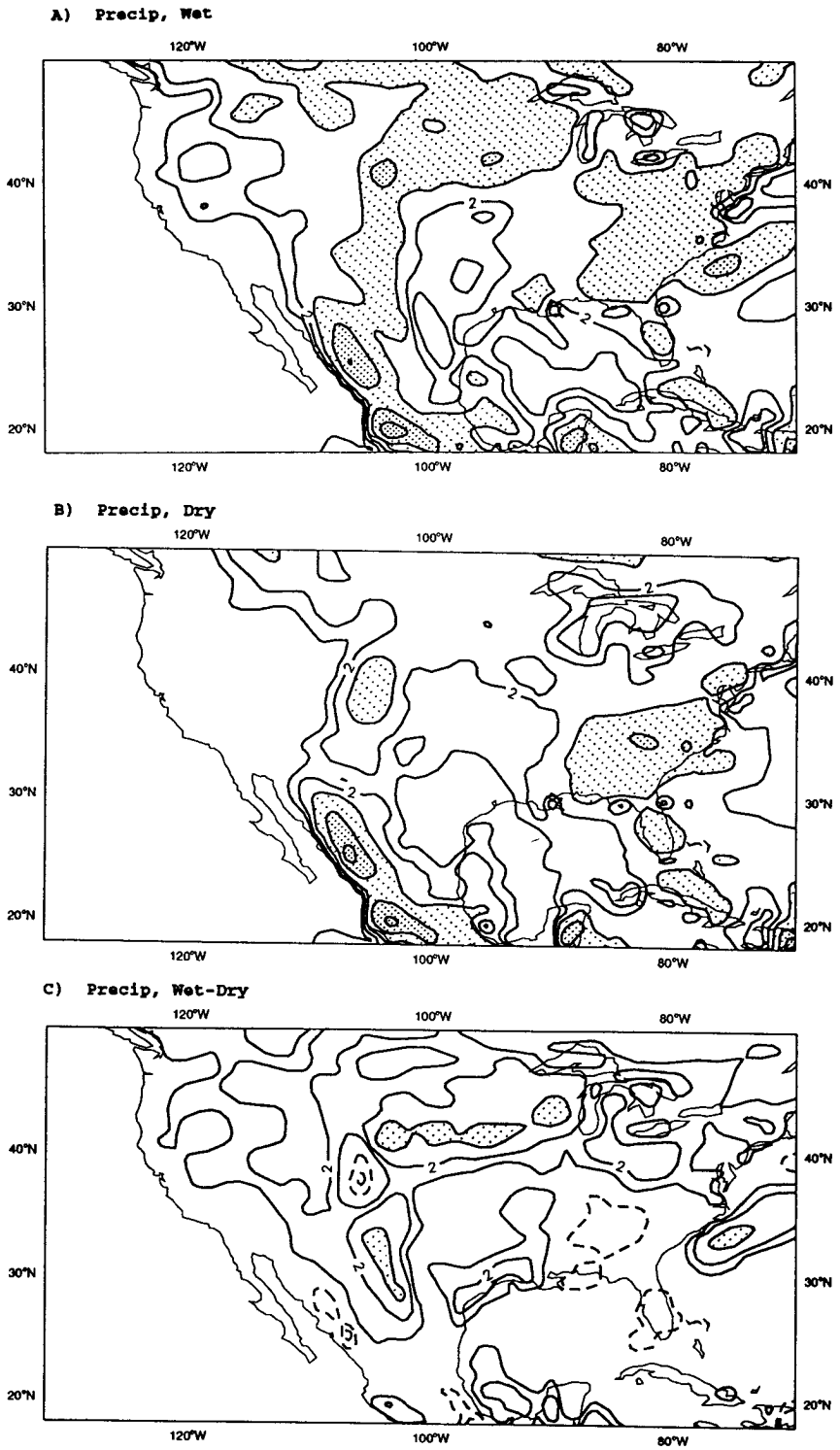

Figure 1: Precipitation averaged over an ensemble of three 30-day forecasts for July 1993 using the ECMWF model. (a) Moist initial soil moisture (field capacity). (b) Dry initial soil moisture (25% availability). (c) Differencebetween moist and dry. Contours are at 1, 2, 4, 8, mm day^{-1} with shading above 4 mm day^{-1}. (From Beljaars et al. (1996).)

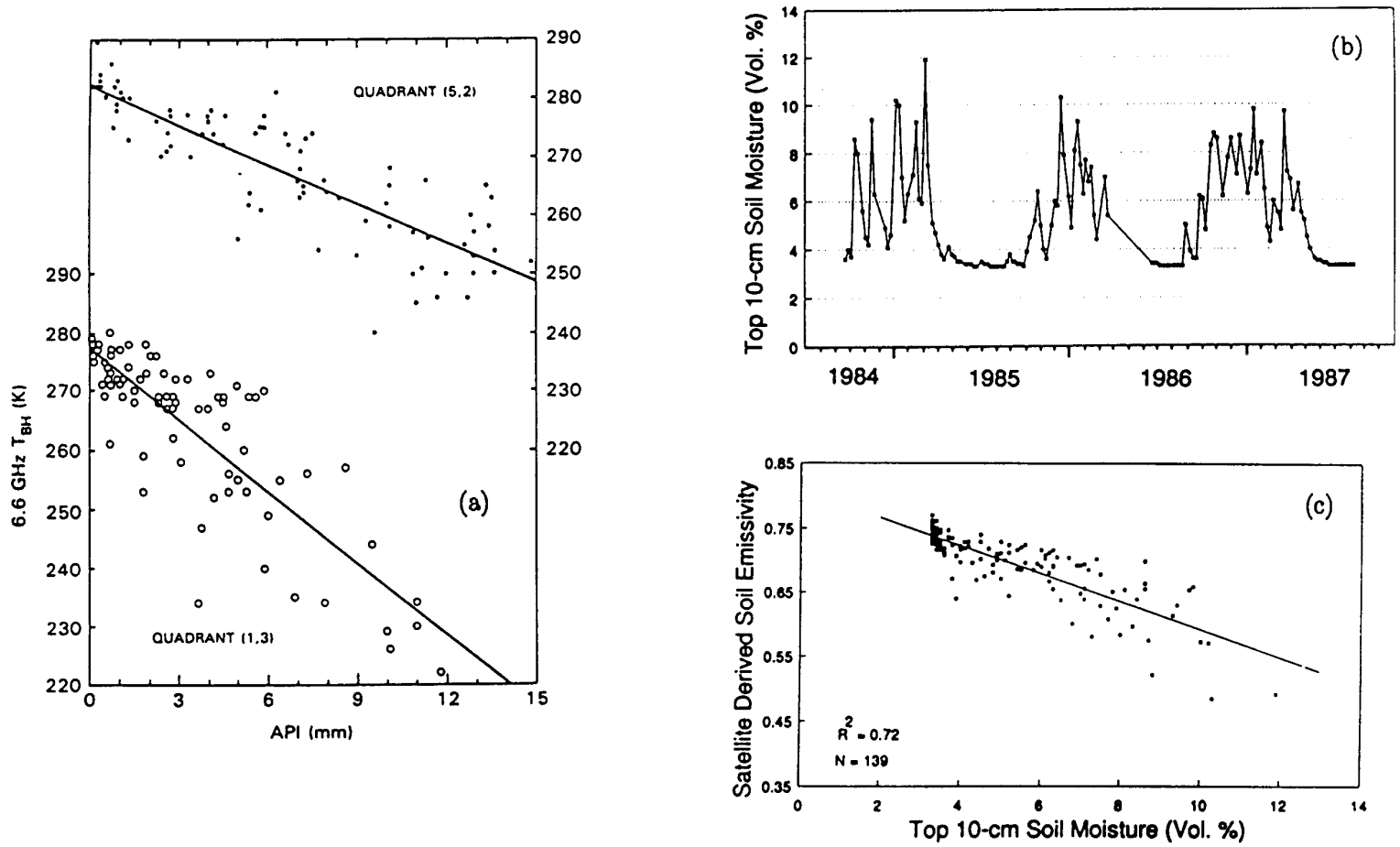

Figure 2: (a) Brightness temperature response to surface moisture (antecedent precipitation index) at 6.6 GHz using SMMR spaceborne observations, for surfaces of different vegetation cover (Choudhury and Golus, 1988). (b) Large-area soil moisture derived from in situ data and soil model for times of SMMR overpasses; and (c) relationship between SMMR-derived surface emissivity and soil moisture after correction for vegetation (van de Griend and Owe, 1994).

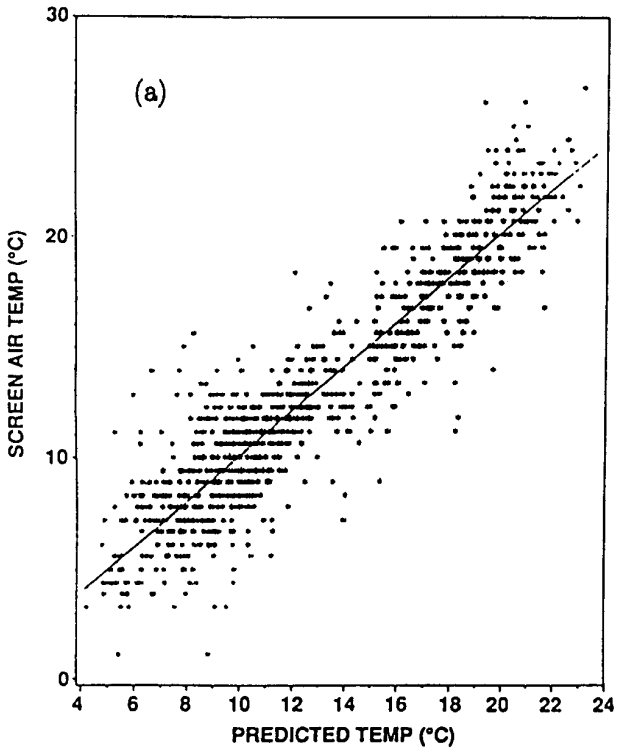

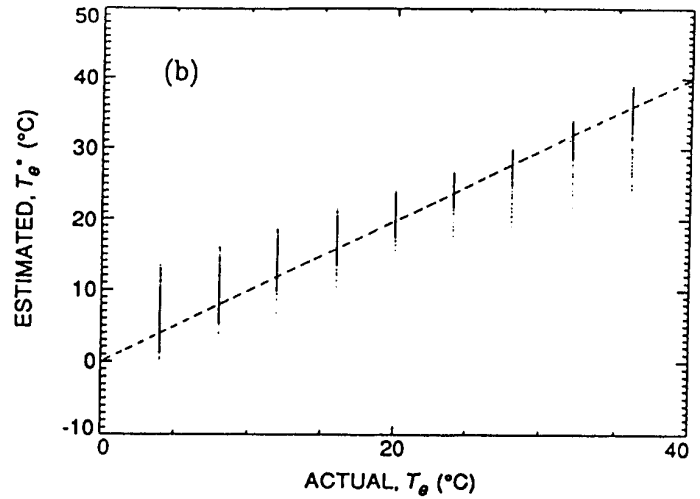

Regression Coefficients and Statistics for 4-Channel Model:

Land Surface Type	R^2	RMSE	Intercept	85 V	37 V	22 V	19 H
Crops/range	0.81	2.58	22.40	1.239	-0.396	0.275	-0.174
Moist soils	0.85	1.99	41.69	1.245	-0.724	0.415	-0.063
Dry soils	0.62	2.60	76.28	-0.367	-0.318	1.408	0.025
All	0.79	2.37	58.07	0.811	-0.555	0.730	-0.170

Figure 3: (a) Surface air temperature versus retrieved land surface temperature using SSM/I observations (McFarland et al., 1990). (b) Simulated linear regression retrievals of land surface temperature, using SMMR, for surfaces including vegetation ranging from 0 to 2 kg m^{-2} water content.

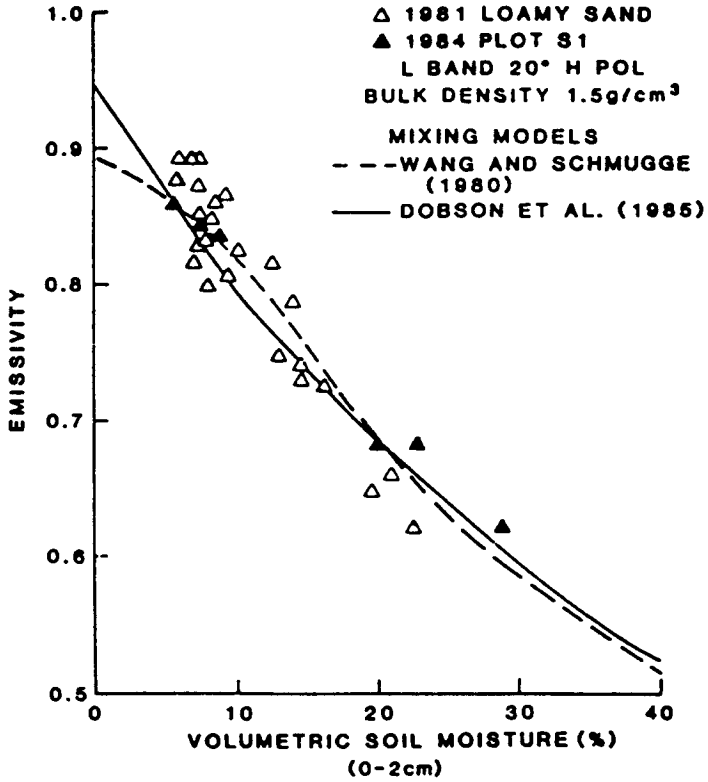

Figure 4: Observed and computed relationships between emissivity an dsoil moisture for bare, smooth fields (loamy sand) at 1.4 GHz. (Jackson and O'Neill, 1987.)

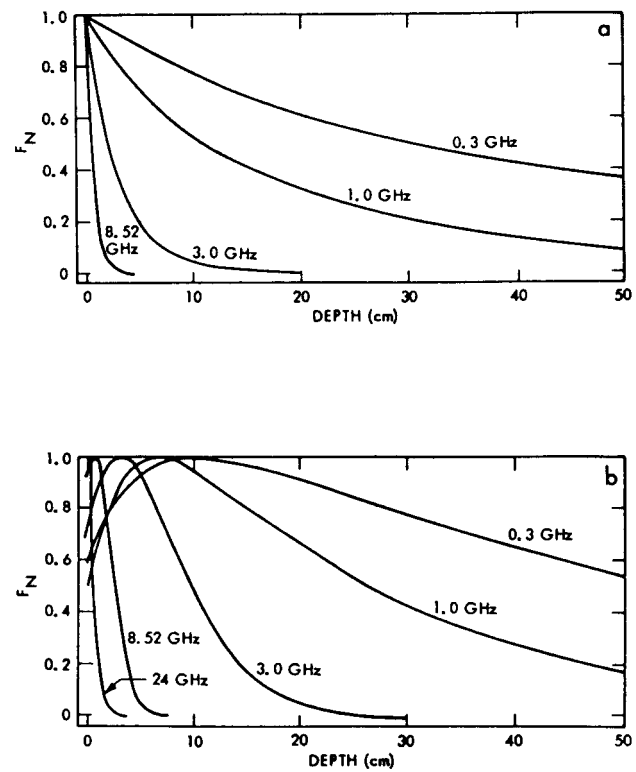

Figure 5: Normalized temperature weighting functions for: (a) wet moisture profile, (b) profile with dry surface and rapidly increasing soil moisture with depth.

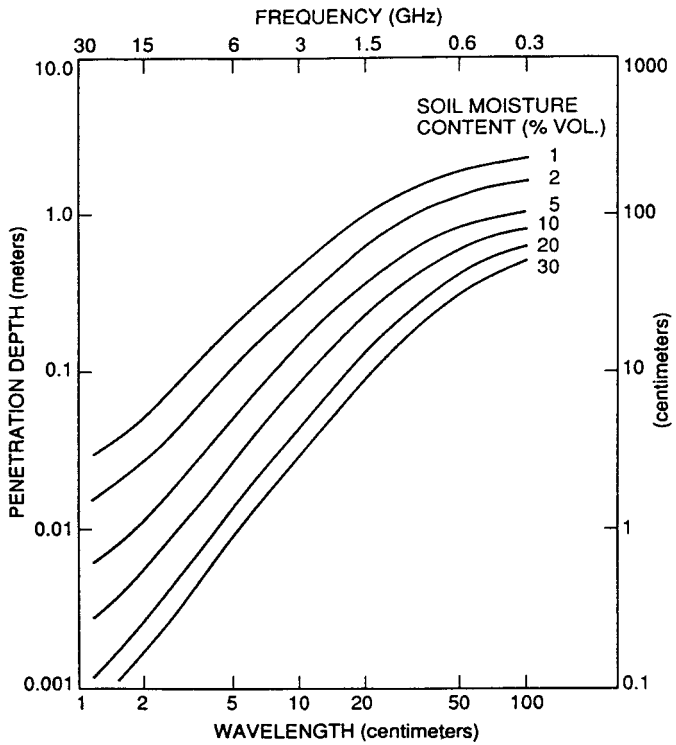

Figure 6: Microwave soil penetration depth as a function of frequency and moisture content.

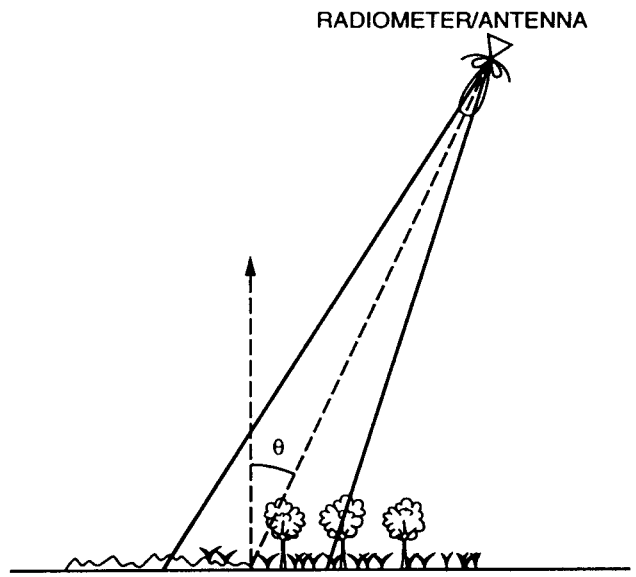

Figure 7: Schematic configuration of a radiometer viewing a heterogeneous scene (bare soil, roughness, vegetation) from a remote platform at viewing angle, θ.

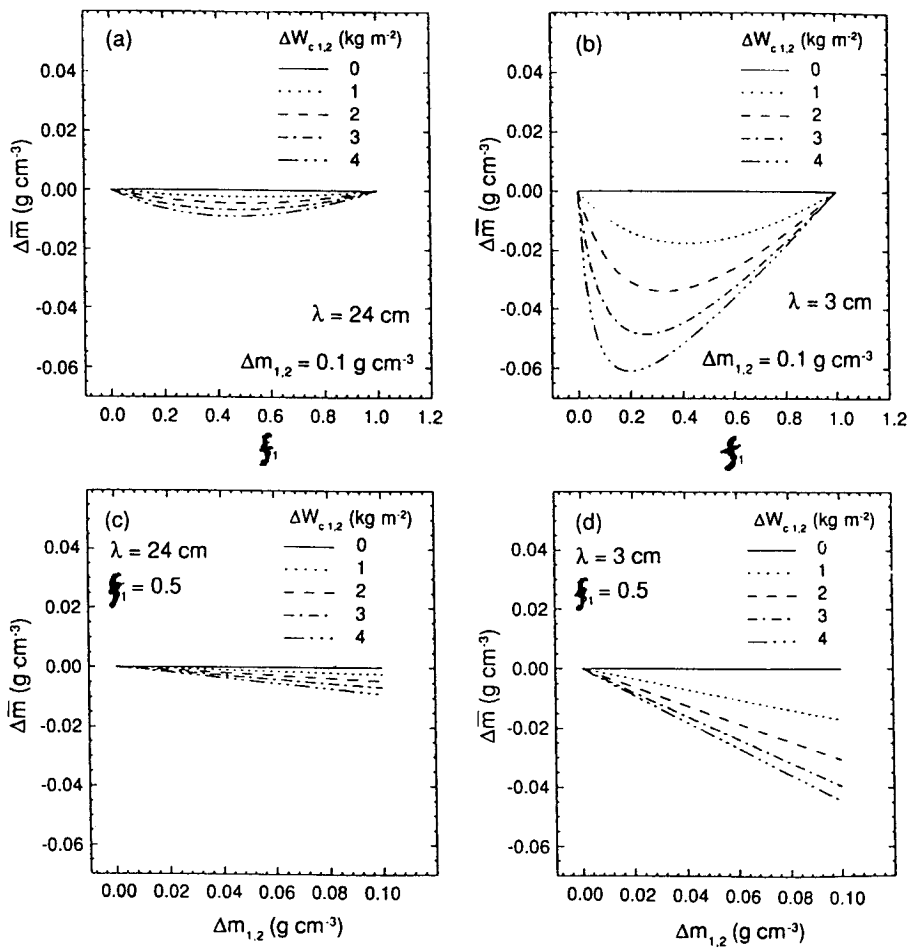

Figure 8: Difference, $\Delta m = m - m'$ (see text), for a two-component surface: (a) as a function of fractional cover, f_1, for soil moisture contrast $\Delta m_{1,2}$ = 0.1 g cm^{-3}, with vegetation water content contrast, $\Delta W_{c1,2}$, as a parameter, and a wavelength of 24 cm; (b) same as (a) but for a wavelength of 3 cm; (c) as a function of soil moisture contrast, $\Delta m_{1,2}$, with vegetation water content contrast, $\Delta W_{c1,2}$, as a parameter, for fractional cover, f_1 = 0.5, and a wavelength of 24 cm; (d) same as (c) but for a wavelength of 3 cm. (Njoku et al., 1995b).